Formation of α-synuclein Lewy neurite–like aggregates in axons impedes the transport of distinct endosomes

Laura A. Volpicelli-Daley[a,b], Karen L. Gamble[c], Christine E. Schultheiss[b], Dawn M. Riddle[b], Andrew B. West[a], and Virginia M.-Y. Lee[b]

[a]Department of Neurology and [c]Department of Psychiatry and Behavioral Neurobiology, University of Alabama, Birmingham, Birmingham, AL 35294; [b]Department of Pathology and Laboratory Medicine, Institute on Aging, and Center for Neurodegenerative Disease Research, University of Pennsylvania School of Medicine, Philadelphia, PA, 19104

ABSTRACT Aggregates of α-synuclein (α-syn) accumulate in neurons in Parkinson's disease and other synucleinopathies. These inclusions predominantly localize to axons even in the early stages of the disease, but their affect on axon function has remained unknown. Previously we established a model in which the addition of preformed α-syn fibrils to primary neurons seeds formation of insoluble α-syn inclusions built from endogenously expressed α-syn that closely recapitulate the neuropathological phenotypes of Lewy neurites found in human diseased brains. Here we show, using live-cell imaging, that immobile α-syn inclusions accumulate in axons from the recruitment of α-syn located on mobile α-syn–positive vesicles. Ultrastructural analyses and live imaging demonstrate that α-syn accumulations do not cause a generalized defect in axonal transport; the inclusions do not fill the axonal cytoplasm, disrupt the microtubule cytoskeleton, or affect the transport of synaptophysin or mitochondria. However, the α-syn aggregates impair the transport of Rab7 and TrkB receptor–containing endosomes, as well as autophagosomes. In addition, the TrkB receptor–associated signaling molecule pERK5 accumulates in α-syn aggregate–bearing neurons. Thus α-syn pathology impairs axonal transport of signaling and degradative organelles. These early effects of α-syn accumulations may predict points of intervention in the neurodegenerative process.

INTRODUCTION

Intracellular pathological amyloid inclusions are a common feature of neurodegenerative diseases. These aggregates accumulate in the soma and throughout axons. In Parkinson's disease (PD) and other synucleinopathies such as dementia with Lewy bodies (DLB)

the axonal accumulation of α-synuclein (α-syn) into amyloid fibrils of distinct morphology, called Lewy neurites (LNs), is particularly abundant relative to Lewy bodies (LBs) in the soma. In brain areas such as the amygdala and striatum, these axonal LNs predominate over perikaryal LBs and appear early in the disease process (Braak *et al.*, 1999, 2003; Duda *et al.*, 2002). Thus axonal accumulation of α-syn as LNs could disrupt axonal transport, compromising neuron function and survival (Salinas *et al.*, 2008; Morfini *et al.*, 2009; Perlson *et al.*, 2010) and thus contributing to neurodegeneration.

Primary neuron models and live-cell microscopy provide the spatial and temporal resolution for the visualization and quantification of organelle transport. The effect of LNs on transport in the neurodegenerative process has been poorly understood because of a lack of suitable primary neuronal models to study this process. For example, in transgenic mouse models overexpressing mutant α-syn, pathological aggregates only form in aged animals, and inclusion formation is coincident with the death of the animals

(Masliah *et al.*, 2000; Giasson *et al.*, 2002; Lee *et al.*, 2002). In addition, primary neurons generated from these transgenic mice do not form α-syn aggregates such as LNs. Overexpression of wild-type (wt) or mutant α-syn through transfection or viral vector transduction also does not form aggregates that faithfully recapitulate the pathological features of LBs/LNs found in diseased synucleinopathy brains.

Our recent development of a novel neuronal α-syn aggregation model in primary neurons provides a major advance in analyzing α-syn aggregate formation that recapitulates many of the features found in diseased brains, such as LNs (Volpicelli-Daley *et al.*, 2011). Addition of α-syn preformed fibrils (PFFs) generated from recombinant α-syn protein to primary neurons seeds the recruitment of normal, endogenously expressed α-syn into pathological aggregates that, similar to LBs and LNs in synucleinopathies, are insoluble, hyperphosphorylated, ubiquitinated, and filamentous by electron microscopy (Volpicelli-Daley *et al.*, 2011). α-Syn aggregates follow a lag phase in which no aggregates are initially detectable, but by 4–7 d, small, insoluble aggregates first form in axons, followed by the formation of somatodendritic α-syn inclusions. Formation of α-syn pathology is accompanied by defects in neuronal synchronization early in the disease process, and cell death occurs weeks after initial α-syn aggregate formation. Thus the temporal and spatial nature of α-syn aggregation allows for the investigation of both early- and late-stage defects caused by LNs, and later both LNs and LBs, at time points well delineated from cell death.

Here we show that formation of axonal LNs leads to early and selective alterations in axonal transport. Whereas the transport of mitochondria and synaptic vesicle precursors remain relatively unimpeded, Rab7-positive and TrkB-positive endosomes, as well as autophagosomes, show major perturbations in transport. We also show that major abnormalities in endosome morphology, autophagosome acidification, and autophagosome/lysosome fusion correlate well with α-syn aggregates. Together these observations contribute to growing evidence implicating abnormalities in endosomes as a mechanism contributing to neurodegeneration in PD.

RESULTS

Previously we showed that high-density neuronal cultures develop α-syn aggregates resembling LNs in the majority of axons treated with exogenously applied α-syn PFFs. To visualize and monitor in real time the templated recruitment of endogenous α-syn into LN-like aggregates in axons, we expressed C-terminally tagged α-syn–green fluorescent protein (GFP) in primary neurons by transfection. For these experiments, we used hippocampal neurons generated from α-syn–knockout (KO) mice, so that all α-syn evaluated represented α-syn–GFP and not endogenous α-syn, which may coaggregate with α-syn–GFP. The expression of α-syn–GFP was approximately equivalent to expression of endogenous α-syn (Supplemental Figure S2A). In addition, phosphate-buffered saline (PBS)–treated and PFF-treated α-syn KO showed no abnormalities in overall neuritic morphology (Supplemental Figure S2B), and neurons lacking α-syn do not have significant changes in synaptic ultrastructure or physiology (Chandra *et al.*, 2004). In control, PBS-treated neurons (i.e., no α-syn PFF exposure), α-syn–GFP (Figure 1, A and C, top left) localized to small puncta in neurites and showed diffuse localization in the neuronal soma. α-Syn–GFP was completely extracted by 1% Triton X-100, as shown previously for endogenous, soluble α-syn (Volpicelli-Daley *et al.*, 2011). In PFF-treated neurons, α-syn–GFP aggregates were found in neurites and soma (Figure 1, A and B) that were morphologically similar to the inclusions formed by PFF-induced recruitment of endogenous (i.e., untagged) α-syn (Volpicelli-Daley *et al.*, 2011). The PFF-induced α-syn–GFP aggregates

remained after extraction with 1% Triton X-100 and thus were insoluble, a defining feature of pathological α-syn aggregates.

Because α-syn-GFP pathological inclusions were biochemically similar to α-syn aggregates formed from unmodified endogenous α-syn, we next determined whether α-syn–GFP in PFF-treated neurons undergoes similar posttranslational modifications, such as phosphorylation and ubiquitination, which characterize LBs and LNs in human brains.. We performed immunofluorescence on 1% Tx-100–extracted neurons using monoclonal antibody (mAb) 81A, which, at high dilutions (1:10,000), recognizes only abnormal, phosphorylated α-syn in PFF-treated cells with minimal background fluorescence in control neurons. In PBS-treated α-syn KO neurons, there was no immunofluorescence signal for phosphorylated α-syn (p-α-syn; Figure 1A). In PFF-treated neurons, insoluble α-syn-GFP aggregates colocalized extensively with mAb 81A (Figure 1A), indicating that the aggregates were phosphorylated. Furthermore, cotransfection of α-syn-GFP with monomeric red fluorescent protein (mRFP)–ubiquitin and live imaging showed that α-syn-GFP inclusions colocalize extensively with ubiquitin (Figure 1B), another feature of LBs and LNs in pathological brain tissue. Thus, similar to endogenous α-syn, PFF treatment causes recruitment of α-syn–GFP, to insoluble phosphorylated and ubiquitinated aggregates that resemble LNs in the axons and LBs in the soma. Moreover, use of α-syn-GFP allows direct visualization of α-syn pathology formation in live neurons.

Having established that α-syn–GFP distribution and recruitment into aggregates are similar to those with endogenous α-syn (Figure 1), we performed live imaging to analyze their growth and mobility. C-terminally tagged axonal α-syn–GFP particles in PBS-treated neurons can undergo fast axonal transport similar to N-terminally tagged GFP–α-syn demonstrated previously (Roy *et al.*, 2007; Figure 1C). However, in neurons 7 d after exposure to PFFs, there was a significant decrease in the percentage of mobile syn-GFP particles in the anterograde direction (Figure 1, C and D). However, the remaining mobile α-syn–GFP vesicles in PFF- treated neurons had similar velocities to PBS-treated neurons (Figure 1E).

When imaged over a more prolonged time course, it was apparent that the larger α-syn–GFP aggregates in PFF-treated neurons remained relatively immobile (Figure 1F and Supplemental Movies S1). However, smaller, mobile α-syn–GFP particles could be seen to travel along the axon and merge with the larger, elongated structures, suggesting recruitment of endogenous α-syn–GFP into the larger accumulations (Figure 1F; arrows indicate mobile vesicles; arrowheads indicate merging of these vesicles with larger aggregates). In addition, smaller α-syn–GFP aggregates can be seen breaking off from and remerging with the larger structures. Overall, these studies provide insights into the temporal and spatial dynamics of the recruitment of endogenous axonal α-syn into LN-like structures in live neurons.

Ultrastructure of inclusions, microtubules, and endosomes

Because the large α-syn–GFP aggregates were relatively immobile, we conducted immuno–electron microscopy (EM) in control PBS- and PFF-treated neurons to determine the spatial relationship between p-α-syn aggregates, membrane organelles, and the cytoskeleton. These experiments were performed in wild-type primary neurons that express α-syn endogenously, since GFP fluorescence was unnecessary. In PBS-treated neurons, microtubules and mitochondria can be seen in axons with (Figure 2A) and without varicosities (Figure 2, B and C). p-α-Syn aggregates in the axons of neurons 14 d after PFF addition (day in vitro [DIV] 19) were visualized using horseradish peroxidase (HRP)–conjugated anti-mouse secondary antibody (Figure 2, D and E) and immunogold (Figure 2, F–I). We
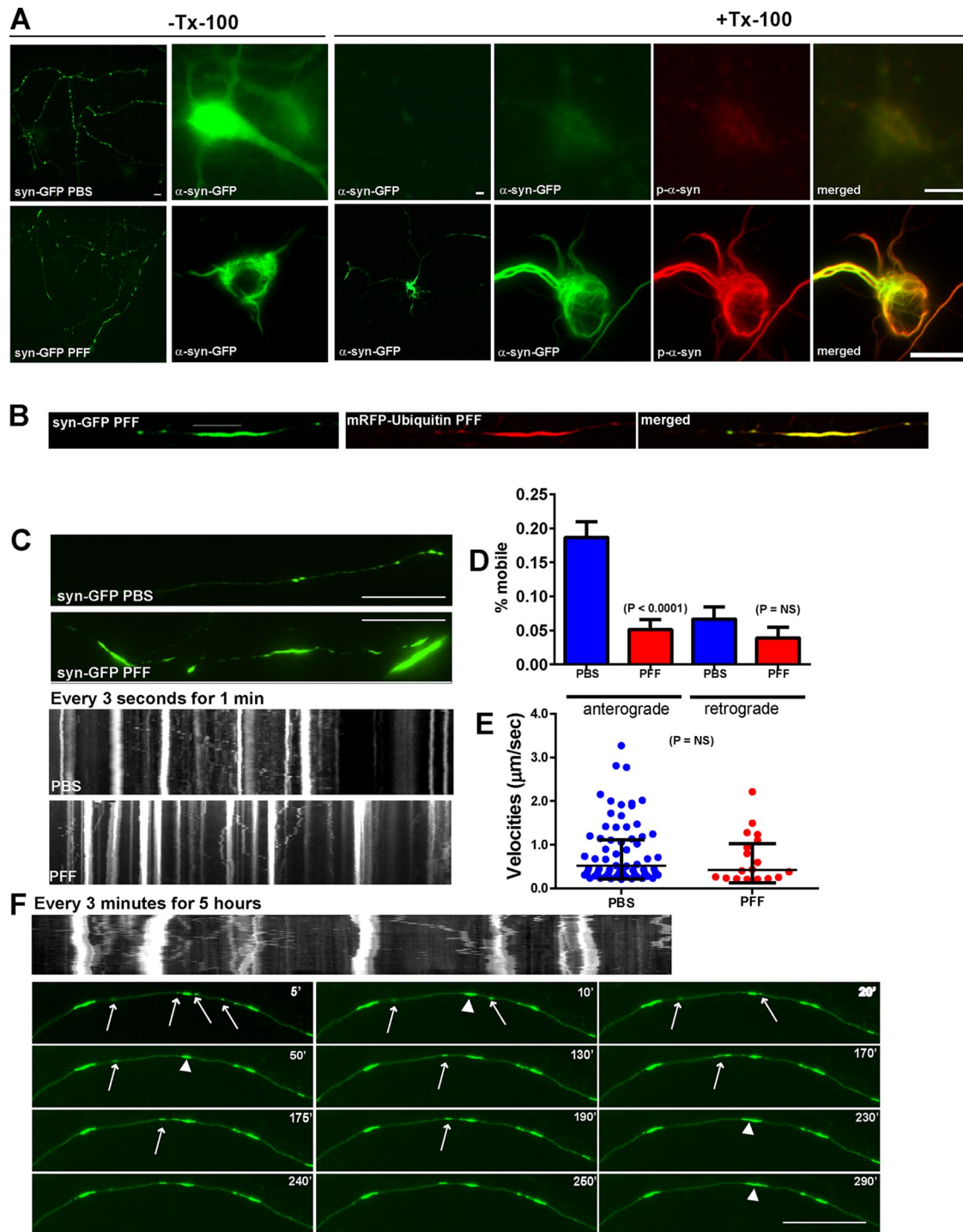
FIGURE 1: PFFs induce formation of α-syn-GFP aggregates that are immobile and grow by recruitment of mobile α-syn vesicular carriers. Primary hippocampal neurons from α-syn KO mice were transfected with α-syn-GFP and treated with PBS or PFFs and imaged 7 d later. Syn-GFP, number of particles analyzed, 484 for PBS and 387 for PFF (18 axons, PBS; 22 axons, PFF). (A) In PBS-treated neurons (top), α-syn-GFP localized to puncta corresponding to presynaptic terminals. α-Syn-GFP was soluble and thus extractable when fixed with paraformaldehyde containing 1% Triton X-100. PBS-treated neurons showed minimal p-α-syn immunoreactivity. Seven days after PFF treatment, α-syn-GFP localized to longer, more serpentine aggregates and small puncta. These aggregates were not extractable with 1% Triton X-100. The insoluble aggregates were extensively phosphorylated, as revealed by immunofluorescence with an antibody specific for p-Ser-129. Scale bar, 50 μm (low magnification), 20 μm (high magnification). (B) Neurons were cotransfected with α-syn-GFP and mRFP-ubiquitin and imaged 7 d post-PFF. Neurons were imaged with the spinning disk confocal, and mRFP-ubiquitin could be seen to coaccumulate with α-syn-GFP aggregates. (C) Live movies of α-syn-GFP were captured every 1 s for 3 min. Top two snapshots show α-syn-GFP in PBS- and PFF-treated neurons. Small axonal puncta were visible in the PBS-treated neurons, whereas longer α-syn-GFP serpentine aggregates were visible in axons from PFF treated neurons. Bottom two kymographs demonstrate that in PBS-treated neurons, there were some mobile and some
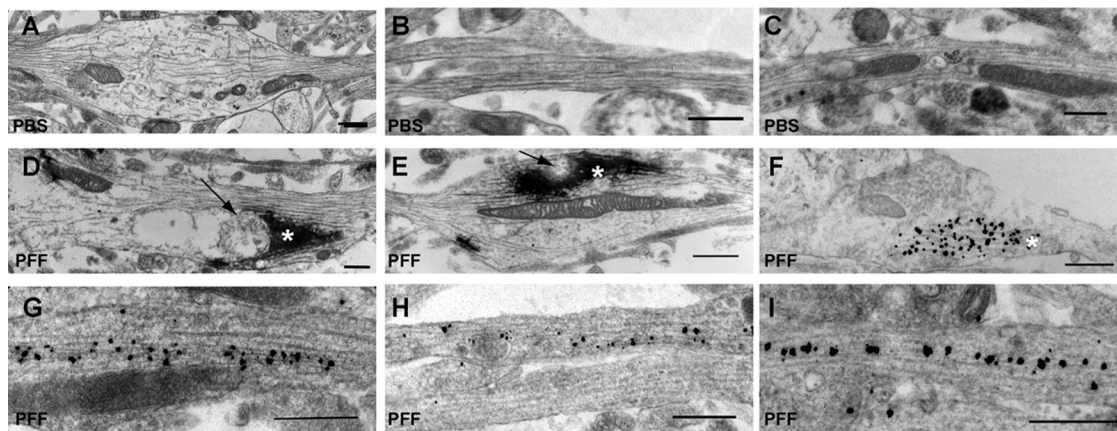
FIGURE 2: Ultrastructure of endosomes in α-syn inclusion–bearing axons. (A, D, E) Immuno-EM of HRP-labeled p-α-syn inclusions in axons. (B, C, F–I) Immunogold-labeled p-α-syn inclusions in axons. (A–C) Three examples of PBS-treated neurons. No HRP immunoreactivity was found in PBS-treated controls. (D–I) Six examples of neurons 14 d after PFF exposure. p-α-Syn aggregates were visible with HRP (asterisks). Immunogold labeling allowed visualization of the 10- to 15-nm filamentous α-syn inclusions. Note that the inclusions did not fill the entire axonal cytoplasm. Arrows point to examples of membrane organelles juxtaposed to the aggregates. Scale bar, 500 nm.

found that the α-syn aggregates did not fill the width of the axonal cytoplasm with (Figure 2, D–F) or without (Figure 2, G–I) varicosities, suggesting that transport of organelles along the axon could occur. For example, mitochondria could be seen adjacent to filamentous accumulations with enough distance between the aggregates and axonal membrane that they could bypass them. In addition, microtubules also appeared intact and thus could potentially support axonal transport (Volpicelli-Daley *et al.*, 2011). These representative images demonstrate that LN-like α-syn aggregates do not necessarily fill the axonal cytoplasm and would be unlikely to sterically hinder or block axonal transport.

α-Syn aggregates do not impair fast axonal transport of synaptophysin or mitochondria

To test the hypothesis that α-syn aggregates do not block axonal transport, we performed live-cell imaging of organelle markers in primary hippocampal cultures derived from wild-type (i.e., nontransgenic) mice expressing endogenous levels of α-syn treated with PBS or α-syn PFFs. Transport of specific organelles was evaluated in mature neurons 7 d after PFF addition (DIV12), when aggregates are apparent in axons throughout the culture but not in the soma or in dendrites and there is no neuron death (Volpicelli-Daley *et al.*, 2011)

Synaptophysin-GFP traversed axons in punctate carriers (Figure 3A). The mobility of these particles appeared similar in control neurons that did not harbor α-syn pathology and PFF-treated neurons bearing axonal LN-like aggregates (PFF-treated; Supplemental Movie S2). There were no significant differences in the percentage of mobile particles between control neurons and neurons harboring

α-syn inclusions (Figure 3B). In addition, there were no significant differences in the abundance of particles per 50 µm of axonal membrane (Figure 3C) or in the number of particle pauses or reversals (Figure 3, D and E). Because the velocities from the PBS- and PFF-treated groups did not fit a normal distribution, a Poisson regression analysis was performed on binned synaptophysin-GFP velocities. This analysis revealed no statistically significant differences between PBS and PFF groups for anterograde or retrograde transport (Figure 3, F and G). Plotting the velocities of mobile vesicles as the median and interquartile range also revealed no differences in the velocities of synaptophysin-GFP in control and α-syn aggregate–bearing axons.

In addition, despite the presence of axonal α-syn aggregates, analyses of transport of a larger organelle such as the mitochondria using yellow fluorescent protein (YFP)–Mito (Figure 4A) revealed no difference between PBS- and PFF-treated groups for percentage of mobile particles (Figure 4B), abundance of YFP-Mito puncta (Figure 4C), number of pauses (Figure 4D), or number of reversals (Figure 4E). In addition, the Poisson regression analysis revealed no significant differences in anterograde or retrograde YFP-Mito velocities (Figure 4, F and G). Thus the presence of α-syn aggregates did not affect transport of synaptophysin or mitochondria.

α-Syn aggregates impair retrograde axonal transport of Rab7 endosomes

Our ultrastructural images showed accumulations of membranous organelles approximately the size and morphology of endosomes near α-syn pathology in axons (see arrows in Figure 2, D and E). Rab7 localizes to endosomes and plays a major role in transport of

immobile α-syn-GFP particles. In the PFF-treated neurons, there appeared to be more immobile particles that were larger in size. The mobile α-syn-GFP particles seem to approach an immobile α-syn-GFP aggregate but not bypass it. Scale bar, 10 µm. (D) Quantified percentage of mobile anterograde and retrograde particles. There was a significant decrease in the percentage of anterograde-moving mobile α-syn-GFP particles in neurons 7 d after PFF treatment. (E) Scatter plot of median velocities of mobile particles with interquartile range. The Mann–Whitney test did not reveal a significant difference between velocities. (F) Neurons expressing α-syn-GFP were treated with PFFs and imaged 7 d later. Images were captured every 3 min over 5 h. The larger aggregates were immobile (arrowheads). Smaller, mobile puncta can be seen to merge with the larger aggregates (arrows). At 240 min, a syn-GFP aggregate can be seen to break away from the larger aggregate, but it remerged at 290 min. Scale bar, 10 µm.
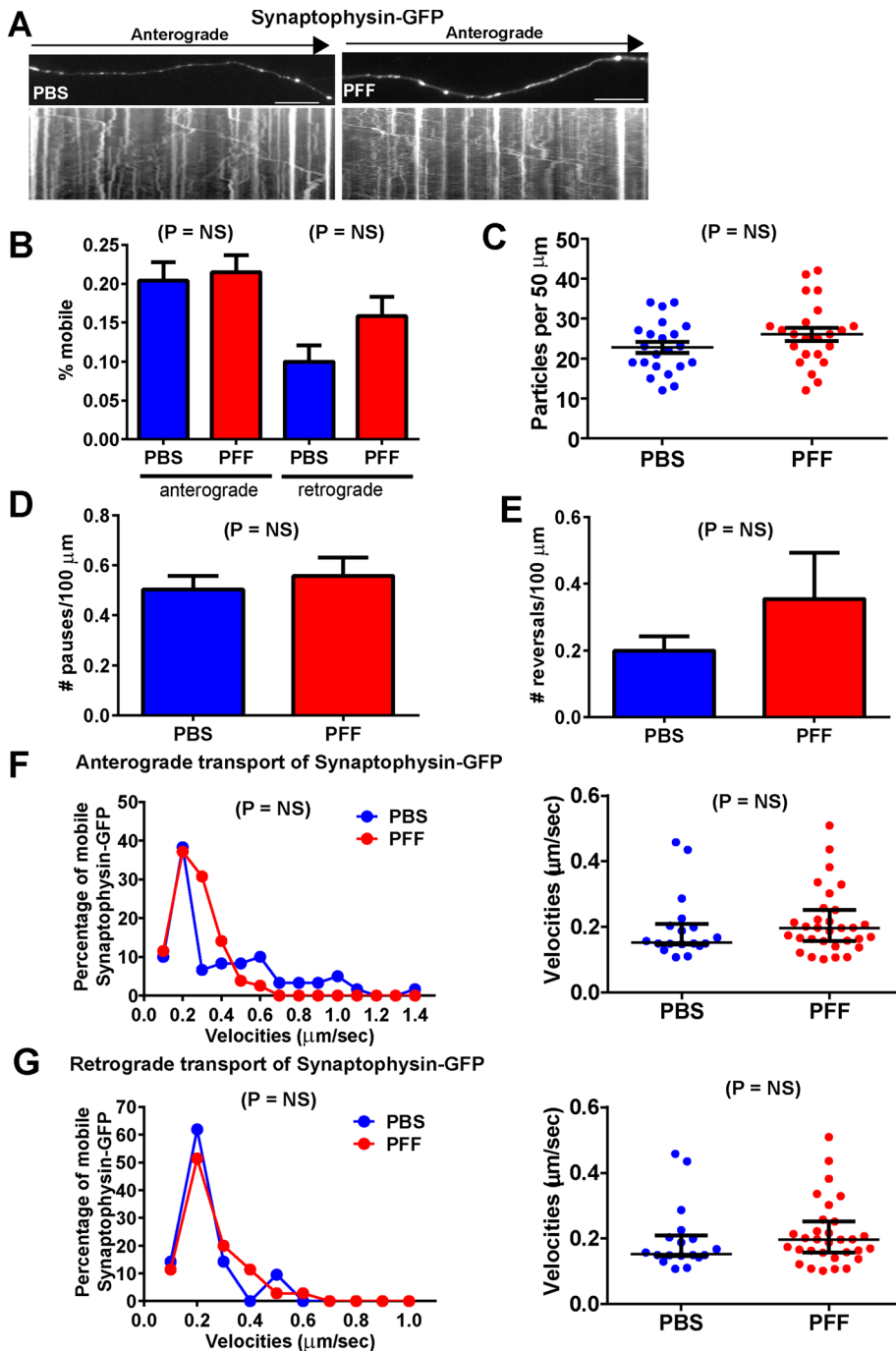
FIGURE 3: Normal transport of synaptophysin-GFP in neurons with α-syn aggregates. Primary hippocampal neurons were transfected with synaptophysin-GFP, treated with PBS or PFFs, and imaged 7 d later. Synaptophysin-GFP, number of particles analyzed, 2044 for PBS and 1944 for PFF (19 axons, PBS; 17 axons, PFF). (A) Top, images from movies captured every 1 s for 3 min; scale bar, 10 μm. Kymographs shown below the images were generated as visual representations of distance traveled over time. (B) Of the mobile particles, the percentages of anterograde and retrograde particles were also quantified. There were no significant differences between the PBS- and PFF-treated groups. (C) There were no significant differences in the mean number of synaptophysin-GFP particles per 50 μm of axonal membrane. In addition, there were no significant differences in the number of pauses (D) or reversals (E) between the two groups. A Poisson regression on velocities binned with 10 cut points was not statistically significant between PBS and PFF groups for anterograde synaptophysin-GFP velocities (Wald χ^2 = 1.420, p = NS; F) or for retrograde synaptophysin-GFP velocities (Wald χ^2 = 3.246, p = NS; G). (F, G) Right, median and interquartile ranges of the velocities of the mobile synaptophysin-GFP particles. The Mann–Whitney test did not produce significant differences for anterograde or retrograde velocities.

these organelles along the axon (Deinhardt et al., 2006). The presence of abnormal α-syn fibrils in axons did not affect the overall mobility of GFP-Rab7 in axons (Figure 5B), the abundance of GFP-Rab7 particles along the membrane (Figure 5C), or the number of pauses (Figure 5D). In addition, a Poisson regression on binned velocities of anterograde traveling particles (Figure 5F) was not statistically significant between PBS and PFF groups However, for retrograde GFP-Rab7 velocities, there was a significant difference between the PBS- and PFF-treated groups (Figure 5G), with a significant reduction in the median velocities in the PFF-treated group. This reduction in velocities could be accounted for by the increase in number of reversals (Figure 5E). Thus the presence of α-syn pathology disrupts the axonal transport of Rab7-positive late endosomes in the retrograde direction.

Dramatically impaired axonal transport of TrkB receptors in α-syn aggregate–bearing neurons treated with brain-derived neurotrophic factor

To determine whether the retrograde transport of other organelles are compromised, we analyzed the movement of TrkB receptors, since these receptors are known to undergo predominantly retrograde axonal transport in endosomes (Deinhardt et al., 2006; Zhou et al., 2012). The most striking change in velocities was found in analysis of retrograde TrkB-GFP transport in brain-derived neurotrophic factor (BDNF)–treated, α-syn inclusion–bearing neurons (Figure 6G and Supplemental Movie S3). Furthermore, the mobility of TrkB-GFP in both the anterograde and retrograde directions also showed significant reductions (Figure 6B), which was reflected by significant increases in the number of pauses (Figure 6D) and reversals (Figure 6E), although the number of particles per 50 μm is unchanged (Figure 6C). In BDNF-treated neurons bearing α-syn inclusions, the velocities of TrkB-GFP showed a significant shift into the lower-velocity bins relative to the control neurons (Figure 6G). In addition, analysis of the median velocities revealed a significant decrease in the neurons exposed to PFFs compared with PBS-treated controls. Images of TrkB-GFP in BDNF-treated neurons with axonal α-syn fibrillar aggregates showed that TrkB-GFP appeared to be localized to more discrete puncta compared with control axons (Figure 6A), possibly reflective of its reduced mobility. The kymographs provide a visual representation of the retrograde movement of TrkB-GFP in BDNF-treated neurons, and it can be seen in both the kymographs and
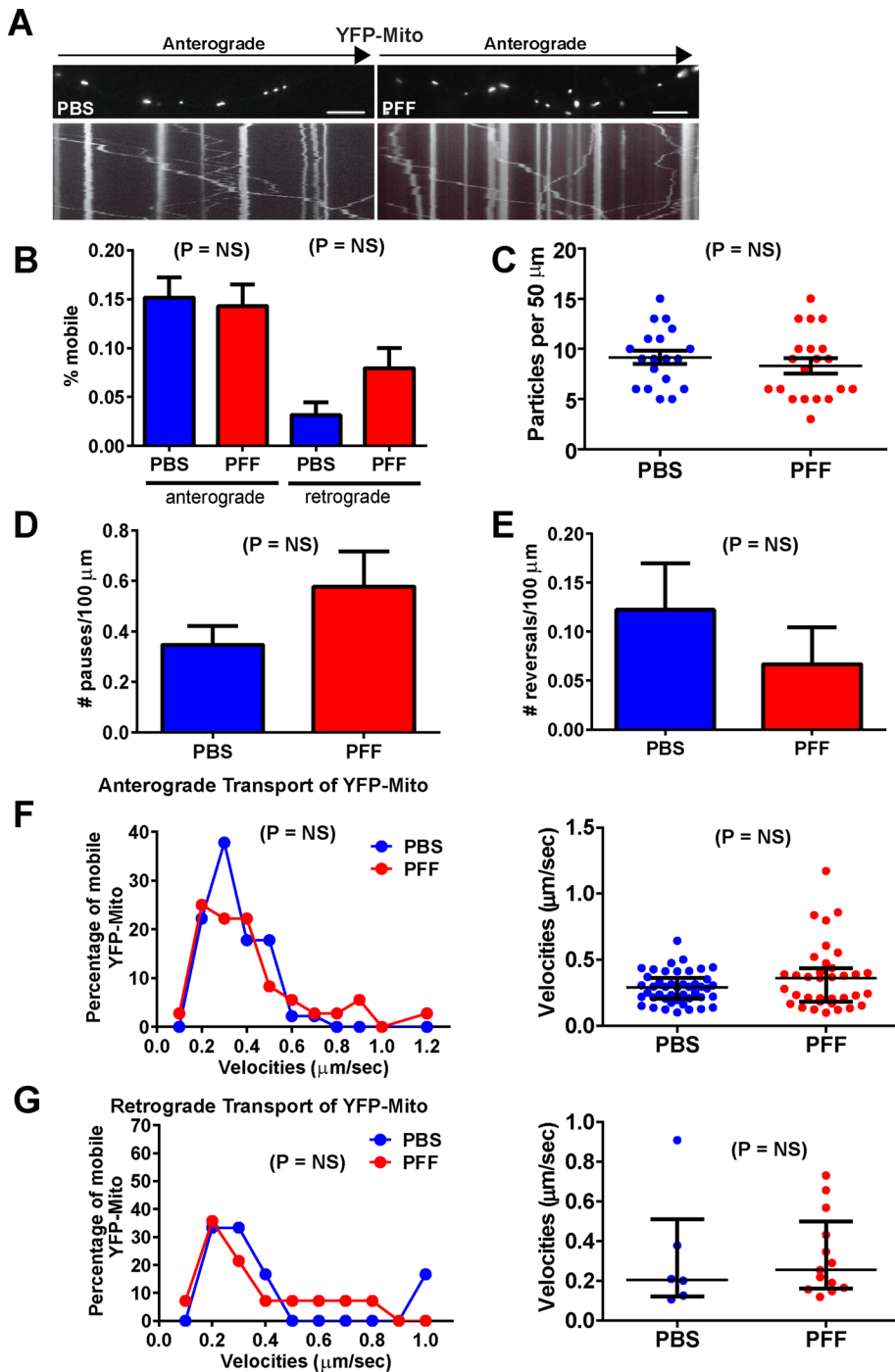
FIGURE 4: Normal transport of YFP-Mito in neurons with α-syn aggregates. Primary hippocampal neurons were transfected with YFP-Mito, treated with PBS or PFFs, and imaged 7 d later. YFP-Mito, number of particles analyzed, 162 for PBS and 244 for PFF (10 axons, PBS; 9 axons, PFF). (A) Top, images from movies captured every 1 s for 3 min; scale bar, 10 μm. Kymographs shown below the images were generated as visual representations of distance traveled over time. (B) Of the mobile particles, the percentages of anterograde and retrograde particles were quantified. There was no significant difference between the PBS- and PFF-treated groups. There were no significant differences in the mean number of YFP-Mito particles per 50 μm of axonal membrane (C), number of pauses (D), or number of reversals (E). A Poisson regression on velocities binned with 10 cut points was not statistically significant between PBS and PFF groups for anterograde YFP-Mito velocities (Wald χ^2 = 0.713, p = NS; F) or for retrograde synaptophysin-GFP velocities (Wald χ^2 = 2.886, p = NS; G). (F, G) Right, median and interquartile ranges of the velocities of the mobile synaptophysin-GFP particles. The Mann–Whitney test did not produce significant differences for anterograde or retrograde velocities.

overall quantitation that there were fewer mobile TrkB-GFP particles in neurons exposed to PFFs with α-syn aggregates.

In neurons not treated with BDNF, there were decreases in the mobility and velocities of TrkB-GFP transport in the PFF-exposed neurons in the retrograde direction (Supplemental Figure S3A). However, there were no significant differences in the number of pauses or reversals or number of particles per unit membrane. There were also no significant differences in the mobility of TrkB-GFP in the anterograde direction. Overall in neurons harboring α-syn aggregates, the mobility of TrkB-GFP retrograde-traveling particles is dramatically slowed, particularly upon BDNF treatment.

Accumulation of TrkB/Rab7 endosomes and pERK5 in α-syn aggregate–bearing neurons

In the soma of control neurons treated with BDNF, TrkB-GFP appeared to localize both to the plasma membrane and intracellular puncta that showed partial overlap with mRFP-Rab7 (Figure 7A). In α-syn aggregate–bearing neurons, TrkB-GFP showed accumulations in enlarged Rab7-positive puncta. Colocalization of TrkB-GFP with mRFP-Rab7 was increased in neurons with abnormal α-syn aggregates (Figure 7B), suggestive of trapping of TrkB receptors in endosomes such that they cannot be targeted to lysosome for degradation. Alternatively, the inability to recycle back to the plasma membrane could also account for this intracellular accumulation.

To provide additional evidence for defective TrkB retrograde transport, we examined the distribution of pERK5, which has been shown to travel with TrkB along the axon to the soma (Watson *et al.*, 2001; Valdez *et al.*, 2005). The immunofluorescence staining for pERK5 in neurons without α-syn aggregates was low (Figure 7C). However, in neurons with α-syn aggregates, p-ERK5 immunofluorescence was more intense and localized to puncta that appeared to be associated with the skein-like α-syn LB-like inclusions in the soma. Thus α-syn aggregates caused both cytosolic accumulation of the TrkB receptor and increase in an associated signaling molecule, pERK5.

Altered autophagosome transport in α-syn aggregate–bearing axons

We also analyzed the transport of autophagosomes, since they are retrogradely transported (Lee *et al.*, 2011; Maday *et al.*, 2012), and we recently showed that the autophagy markers LC3II and p62 increase in expression and colocalize with PFF-induced α-syn
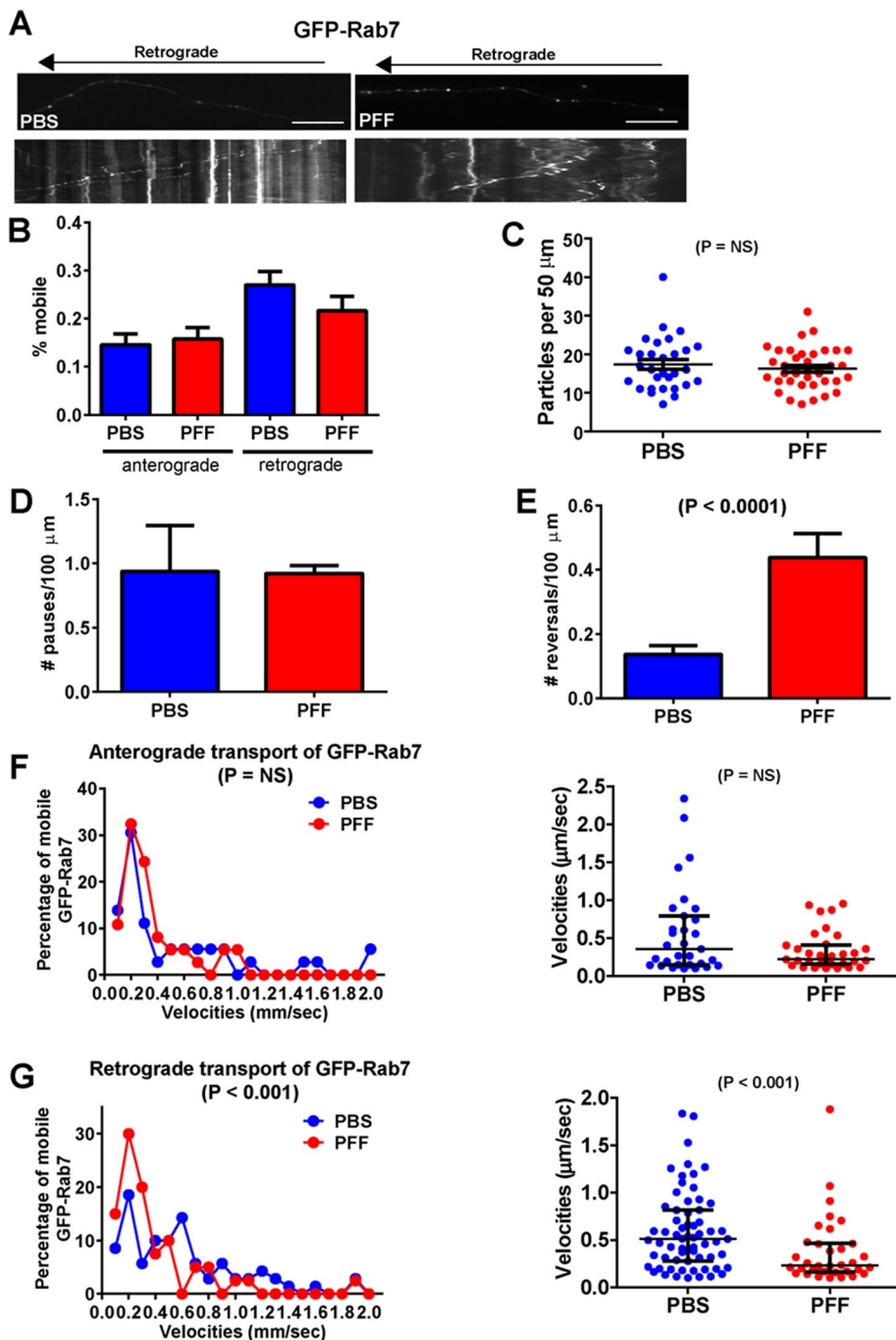
FIGURE 5: Reduced retrograde transport of GFP-Rab7–positive late endosomes in neurons with α-syn aggregates. Primary hippocampal neurons were transfected with GFP-Rab7, treated with PBS or PFFs, and imaged 7 d later. Rab7, number of particles analyzed, 260 for PBS and 179 for PFF (19 axons, PBS; 24 axons, PFF). (A) Top, images from movies captured every 1 s for 3 min; scale bar; 10 μm. Kymographs shown below were generated as visual representations of distance traveled over time. (B) Of the mobile particles, the percentages of anterograde and retrograde particles were quantified. There was no significant difference between the percentages of mobile particles between PBS- and PFF-treated groups. There was no significant difference in the mean number of GFP-Rab7 particles per 50 μm of axonal membrane (C) or number of pauses (D). There was, however, a significant increase in the number of reversals (E). (F) A Poisson regression on velocities binned with 10 cut points was not statistically significant between PBS and PFF groups for anterograde GFP-Rab7 velocities (Wald $\chi^2 = 2.316$, p = NS). Right, median and interquartile ranges of the velocities of the mobile GFP-Rab7 particles. The Mann–Whitney test did not produce significant differences for anterograde velocities. (G) For retrograde GFP-Rab7 velocities, there was a statistically significant difference between the PBS- and PFF-treated groups (Wald $\chi^2 = 13.1$, $p < 0.001$). The odds ratio of 1.30 indicates that

aggregates, concomitant with impairment of autophagy (Tanik et al., 2013). Thus we asked whether the axonal transport of autophagosomes is altered using GFP-LC3 (Figure 8). There was a significant decrease in the overall mobility of GFP-LC3 in neurons harboring α-syn aggregates in both the anterograde and retrograde directions (Figure 8, A and B). There were no changes in the overall abundance of GFP-LC3 particles within the axons of α-syn aggregate–bearing neurons (Figure 8C) or in the number of pauses (Figure 8D) or reversals (Figure 8E). However, of the GFP-LC3 particles that remained mobile, there was an increase in their velocities in both the anterograde and retrograde directions (Figure 8, F and G). This can be seen in the kymographs (Figure 8A); there was an increase in immobile GFP-LC3 autophagosomes in neurons bearing α-syn aggregates, but the autophagosomes that do move, do so rapidly.

α-Syn aggregates alter endosome morphology and autophagolysosome acidification and fusion

What is the fate of the autophagosomes once they reach the neuronal soma? We previously demonstrated an increased abundance of autophagy markers in HEK293 cells with α-syn aggregates and that Lamp1-positive late endosomes/lysosomes are dramatically enlarged, suggesting that autophagosome/lysosome fusion is likely impaired (Tanik et al., 2013). Autophagosomes can merge with Lamp1-positive late endosomes/lysosomes to form autophagolysosomes in which autophagy substrates are degraded (Xie and Klionsky, 2007). We confirmed that Lamp1-positive endosomes/lysosomes were also enlarged in primary neurons (Figure 9, A, B, and D). In PBS-treated neurons, Lamp1 appeared as small puncta throughout the cytoplasm. In neurons with axonal α-syn accumulations, small Lamp-1 puncta were still apparent, but a population of enlarged, Lamp1-positive endosomes appeared. The scatter plot presented in Figure 9D demonstrates an increase in the abundance of larger Lamp1-positive endosomes.

Ultrastructural analysis confirmed abnormalities of endosome morphology in α-syn pathology–bearing axons. Figure 9B shows

the PBS-treated group is 30% more likely to be in the higher-velocity group. Right, median and interquartile ranges of the velocities of the mobile GFP-Rab7 particles. The Mann–Whitney test was significantly different for retrograde velocities.
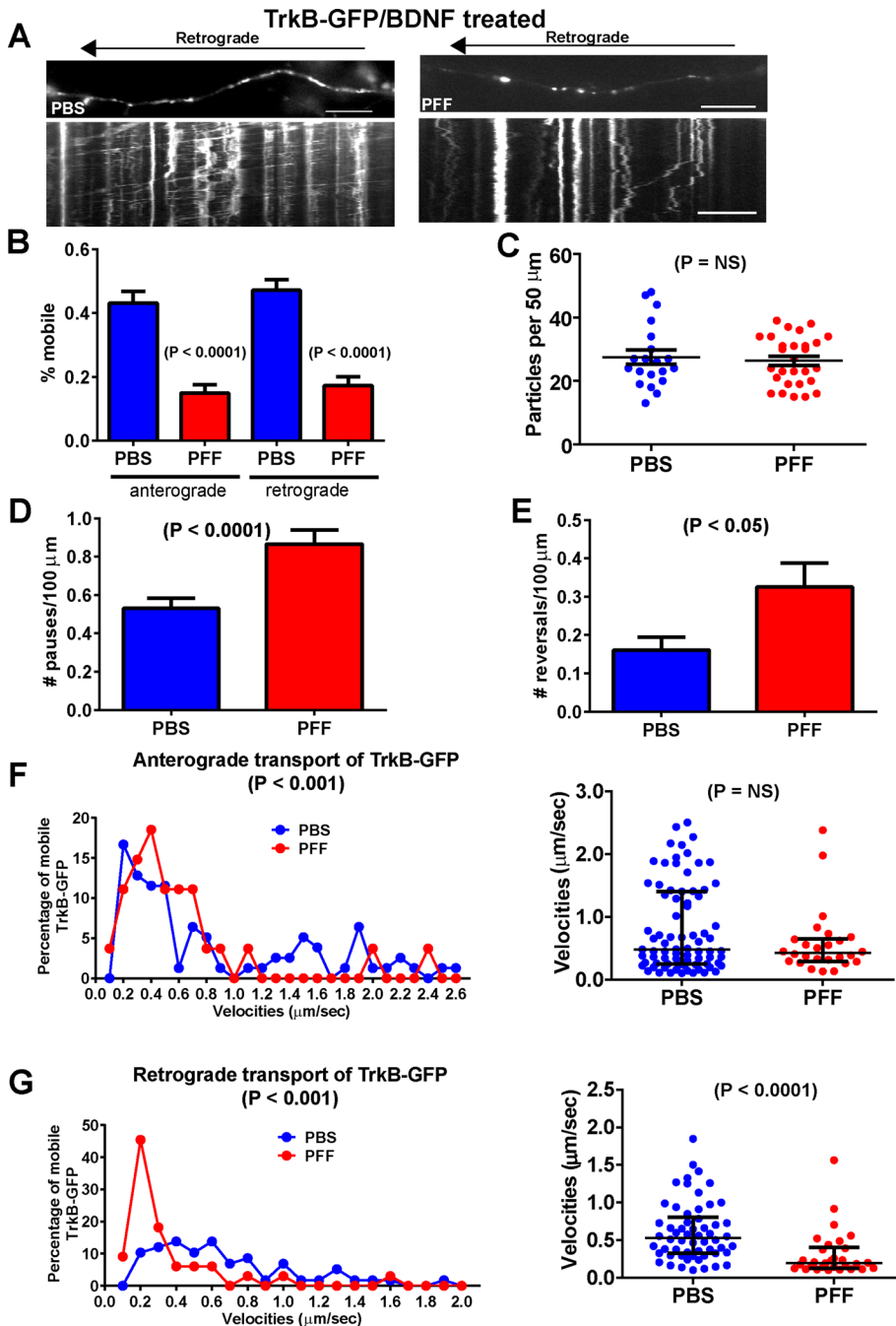
FIGURE 6: Reduced transport of TrkB receptor in BDNF-treated neurons. Primary hippocampal neurons were transfected with TrkB-GFP and imaged 7 d after PBS or PFF addition. Images were captured every 1 s for 3 min. Neurons were treated with BDNF for 30 min before imaging, and BDNF was included in the imaging media. BDNF-treated cultures: TrkB, number of particles analyzed, 453 for PBS and 416 for PFF (19 axons, PBS; 17 axons, PFF). (A) Top, images from movies captured every 1 s for 3 min; scale bar, 10 μm. Kymographs shown below were generated as visual representations of distance traveled over time. (B) Of the mobile particles, the percentages of anterograde and retrograde particles were quantified. There was a significant difference between the percentage of mobile particles between PBS- and PFF-treated groups for particles traveling in both the anterograde and retrograde directions. (C) There was no significant difference in the mean number of TrkB-GFP particles per 50 μm of axonal membrane. Neurons with α-synuclein inclusions showed a significant increase in (D) the number of pauses and (E) the number of reversals. (F) A Poisson regression on velocities binned with 10 cut points was statistically significant between PBS and PFF groups for anterograde TrkB-GFP velocities (Wald $\chi^2 = 61.65$, $p < 0.0001$). The odds ratio of 1.83, indicates that the PBS-treated group is 83% more likely to be in the higher-velocity group. Right, median and interquartile ranges of the anterograde velocities of the mobile TrkB-GFP particles in BDNF-

a late endosome in a control neuron, with its characteristic limiting membrane and internal vesicles of uniform diameter (arrowhead). In PFF-treated neurons with α-syn pathology, the late endosome was enlarged and devoid of uniform internal vesicles (Figure 9B, arrowhead). Moreover, abnormal endosomes with nonuniform internal vesicles could also be seen embedded within p-α-syn–positive aggregates (Figure 2, B and C, arrows).

Because abnormal endosome morphology could reflect functional defects in these organelles, we used a mCherry-GFP-LC3 construct (Kimura *et al.*, 2007) to probe more directly defects in late/endosome lysosome acidification in α-syn fibril–bearing neurons (Figure 9C). When LC3 enters late endosomes/lysosomes, the acidic environment of these organelles quenches the GFP, whereas the mCherry remains visible. This was the case in PBS-treated, non–aggregate-bearing neurons, since the mCherry tag of LC3 is visible as puncta in the soma, but because LC3 is in an acidic environment, the fluorescence from the GFP tag is faint and diffuse (Figure 9C). However, in PFF-treated neurons bearing axonal α-syn pathology, the GFP fluorophore remained bright, with a punctate or vacuolar appearance typical of late endosomes/lysosomes, indicative of impaired endosome/lysosome acidification. Finally, we examined the overlap of LC3 autophagosomes with LAMP1 late endosomes/lysosomes. The amount of colocalization between the two markers was reduced in neurons with α-syn inclusions (Figure 9E). These data suggest that there is a defect in the fusion of autophagosomes with late endosomes/lysosomes.

DISCUSSION

A common defining feature of most neurodegenerative diseases is the formation of insoluble, amyloid protein aggregates. In particular, the accumulation of α-syn filamentous structures as LNs in axons or as LBs in somatodendritic compartments is a predominant feature of PD and synucleinopathies

treated neurons (Mann–Whitney test, $p =$ NS). (G) For retrograde TrkB-GFP velocities in BDNF-treated neurons, there was a statistically significant difference between the PBS- and PFF-treated groups (Wald $\chi^2 = 73.3$, $p < 0.0001$). The odds ratio of 2.48 indicates that the PBS-treated group was 148% more likely to be in the higher-velocity group. The scatter plot on the right shows a striking decrease in the velocities of mobile vesicles, and the Mann–Whitney U test revealed a statistically significant decrease ($p < 0.0001$).
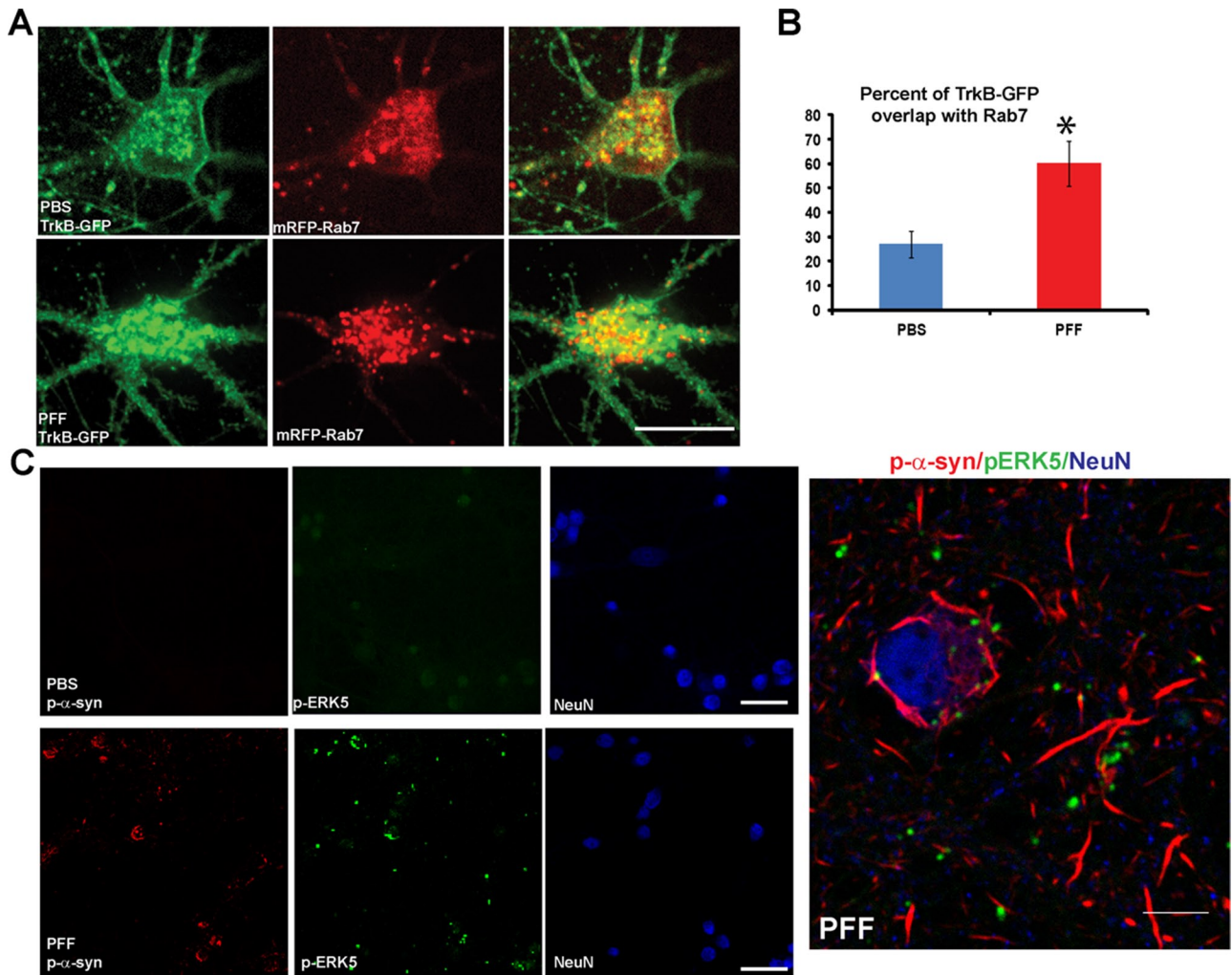
FIGURE 7: Accumulation of endosomes and endosomal-associated signaling molecules in neurons with α-syn aggregates. (A) Neurons were cotransfected with TrkB-GFP and mRFP-Rab7 and imaged by confocal microscopy. Neurons were treated with BDNF for 30 min before imaging. TrkB-GFP appeared to localize at or near plasma membrane and intracellular puncta in neuronal soma of control neurons. In α-syn aggregate–bearing neurons, TrkB-GFP did not appear to localize to the plasma membrane but showed enlarged intracellular accumulations. Scale bar, 10 μm. (B) The percentage of colocalization of TrkB-GFP with mRFP-Rab7 late endosomes was significantly increased in PFF-treated neurons ($t = 3.3$, $p = 0.004$). Scale bar, 10 μm. (C) Neurons (in this case, not transfected with TrkB-GFP or other plasmid) were treated with PBS or PFFs and fixed 7 d later. Immunostaining was performed with antibodies to p-ERK5, p-α-syn, and NeuN as a marker for neuronal soma. Neurons were imaged by confocal microscopy. In control neurons, p-ERK5 showed minimal immunofluorescence. In α-syn aggregate–bearing neurons, p-ERK5 showed increased immunofluorescence and localized to perinuclear puncta juxtaposed to p-α-syn aggregates. Right, higher-magnification image shows that pERK5 puncta can be found juxtaposed to the α-syn aggregates. Scale bar, 10 μm.

(Braak *et al.*, 1999, 2003; Duda *et al.*, 2002). However, because α-syn pathology develops concomitant with the loss of normal localization of endogenous α-syn, it has been difficult to determine the contribution of α-syn aggregates and loss of normal α-syn function in PD pathogenesis. Indeed, beneficial effects of α-syn aggregates have been reported in which such aggregates may sequester numerous soluble toxic species and provide neuroprotection, at least in the short term (Kopito, 2000; McNaught *et al.*, 2002; Kramer and Schulz-Schaeffer, 2007). On the other hand, insoluble aggregates may themselves represent the toxic and transmissible species, with their formation and spread directly responsible for the neurodegenerative phenotypes. Part of the problem in elucidating the role of α-syn pathology has been the lack of model systems with which to study the acute effects of α-syn aggregation occurring in real time in individual neurons. Here we were able to use a recently developed neuron-based culture system and begin to unravel how neuron functionality is affected during the process of α-syn aggregation.

Cumulatively the most conspicuous phenotype in PFF-treated neurons is the accumulation of large LN-like α-syn aggregates in axons, which would be suggestive of impairment of axonal transport. Impaired axonal transport has been implicated in neurodegenerative diseases such as Huntington's disease, amyotrophic lateral sclerosis, and motor and sensory neuropathies, but a role in PD pathogenesis has been less clear (Perlson *et al.*; Salinas *et al.*, 2008; Morfini *et al.*, 2009). We found that axonal transport of organelles such as synaptic vesicle precursors and mitochondria remains normal. Moreover, our ultrastructural analysis demonstrates that α-syn aggregates do not occlude the axon or cause a disruption in the
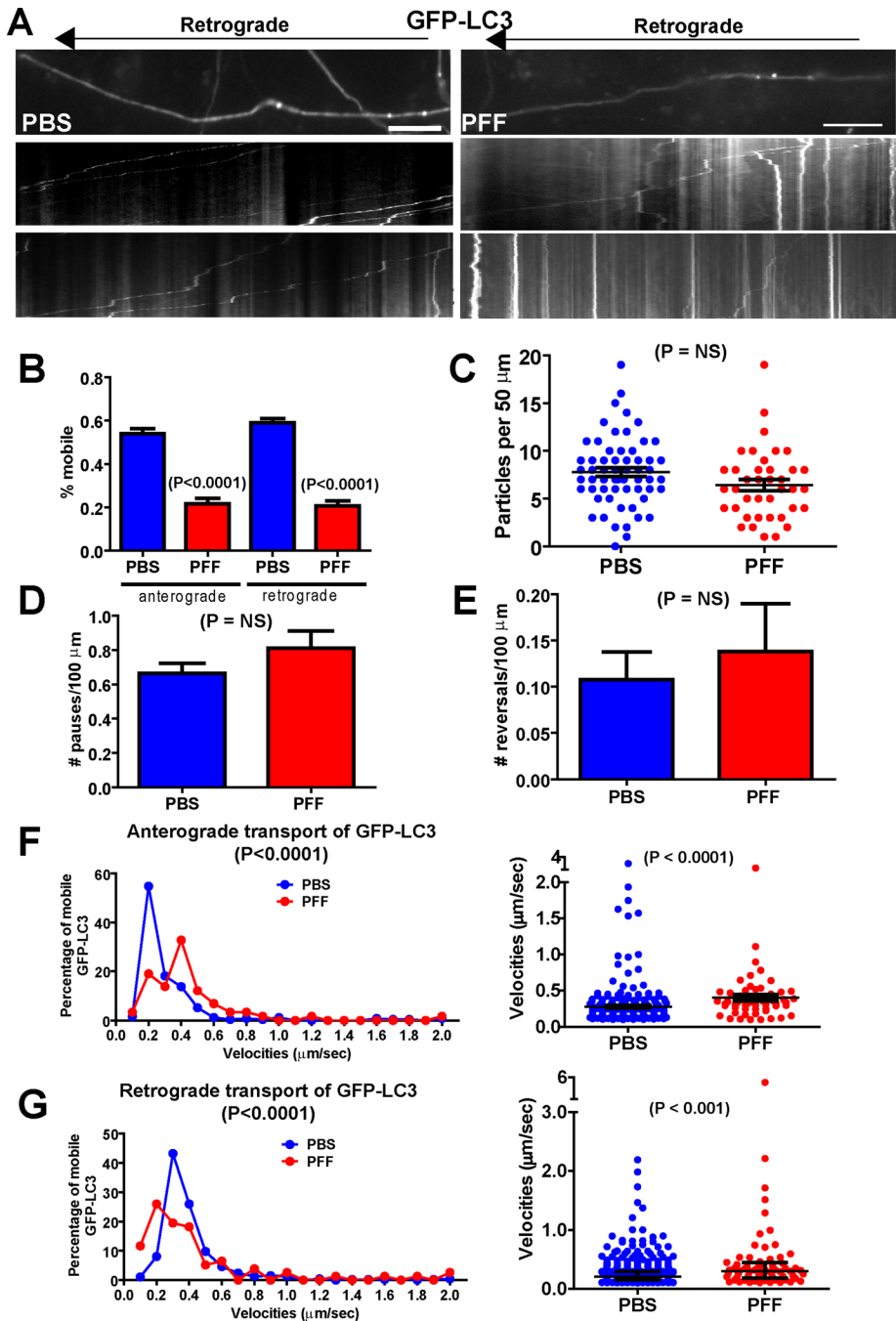
FIGURE 8: Altered transport of GFP-LC3 autophagosomes. Primary hippocampal neurons were transfected with GFP-LC3, treated with PBS or PFFs, and imaged 7 d later. (A) Top, images from movies captured every 1 s for 3 min; scale bar, 10 μm. Kymographs shown below were generated as visual representations of distance traveled over time and used to calculate average velocities as distance traveled over time. Two examples of kymographs generated from independent movies. LC3, number of particles analyzed, 571 for PBS and for 341 PFF (50 axons, PBS; 30 axons, PFF). (B) Percentages of mobile, anterograde and retrograde GFP-LC3 velocities. The Mann–Whitney test revealed significant decreases in the percentage of mobile GFP-LC3 particles in the PFF-exposed neurons. There was no significant difference in the number of GFP-LC3 particles per 50 μm of axonal membrane (C) in PBS- vs. PFF-treated neurons or in number of pauses (D) or number of reversals (E). (F) A Poisson regression on velocities binned with 10 cut points was statistically significant between PBS and PFF groups for anterograde GFP-LC3 velocities (Wald $\chi^2 = 15.98$, $p < 0.0001$). The scatter plot on the right shows the median and interquartile range of the velocities of the anterograde GFP-LC3 particles. The y-axis is broken to help visualize the entire range of velocities. The Mann–Whitney test revealed a statistically significant increase in the velocities of the anterograde GFP-LC3 particles. (G) For retrograde GFP-LC3 velocities, the Poisson regression revealed a statistically significant

microtubule cytoskeleton, demonstrating that some aspects of axonal transport can remain normal. However, we found impairments in endosome and autophagosome transport in α-syn aggregate–bearing axons. Our EM images also show membranous organelles with the morphology of endosomes embedded in the aggregates, reminiscent of early neuropathological analyses of PD brains showing accumulations of membrane vesicles near LBs and accumulations of autophagic vesicles along the axon (Duffy and Tennyson, 1965; Forno and Norville, 1976; Watanabe et al., 1977; Hayashida et al., 1993). Taken together, these data implicate selective defects in endosome/ autophagosome transport and impaired function of these organelles as a major pathogenic event caused by α-syn inclusions in the etiology of PD and other synucleinopathies.

TrkB receptor–containing endosomes show the most robust decrease in axonal transport in α-syn aggregate–bearing neurons. The TrkB receptor travels via endosomes from the presynaptic terminal to the neuronal soma (Deinhardt et al., 2006; Zhou et al., 2012). Retrograde transport of TrkB and other growth factor receptors and associated signaling molecules such as activated pERK5 is important for neuronal survival (Watson et al., 2001; Valdez et al., 2005). Thus slowed transport of TrkB and accumulation of pERK5 in the cytoplasm of α-syn aggregate–bearing neurons may cause defects in signaling pathways crucial for survival, which could lead to cell death. Indeed, pathological studies show accumulation of p-ERK signaling molecules near LBs in PD and DLB brains (Ferrer et al., 2001), confirming that our findings in primary neurons may be relevant for disease. Furthermore, treatment with growth factors has been suggested for PD, but with minimal success (Lewis and Standaert, 2010; Decressac et al., 2012). Our findings suggest a potential mechanism by which the effectiveness of growth factor treatments may be diminished.

In addition to defects in TrkB receptor– and Rab7-positive endosome transport, the axonal mobility of axonal autophagosomes

difference between the PBS- and PFF-treated groups, (Wald $\chi^2 = 18.84$, $p < 0.0001$). The scatter plot on the right shows the median and interquartile range of the velocities of the anterograde GFP-LC3 particles. The y-axis is broken to help visualize the entire range of velocities. The Mann–Whitney test revealed a statistically significant increase in the velocities of the anterograde GFP-LC3 particles.
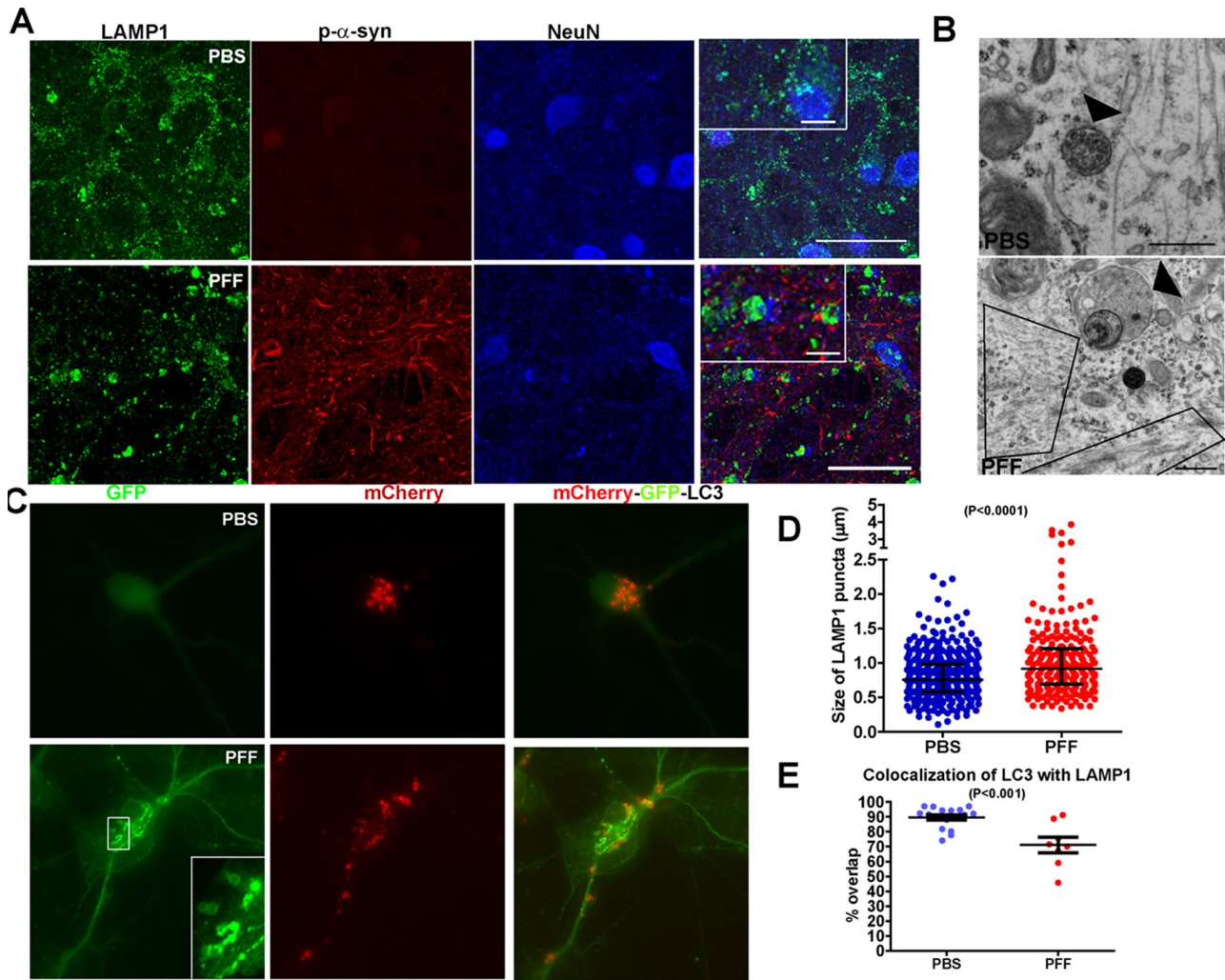
FIGURE 9: Abnormal endosome morphology and autophagosome acidification in α-syn aggregate–bearing neurons. Neurons were treated with PBS or PFFs and fixed 7 d later. (A) Neurons were immunostained with antibodies to the late endosome marker Lamp1, p-α-syn, and NeuN, a marker of neuronal nuclei. Laser-scanning confocal microscopy was performed. In control neurons, Lamp1 appears as small puncta, but in neurons with p-α-syn aggregates, Lamp1-enlarged vacuoles also were visible. Scale bar, 10 μm. (B) Transmission EM was performed on neurons 7 d post PBS or PFF treatment to visualize the ultrastructure of late endosomes (arrowhead). In control neurons, late endosomes show a characteristic limiting membrane, with internal vesicles of uniform size. In PFF-treated neurons, the late endosomes appeared enlarged, with abnormal internal vesicles. The boxes highlight filamentous α-syn inclusions. Scale bar, 500 nm. (C) Neurons were transfected with a mCherry-GFP-LC3 construct, treated with PBS or PFFs, and fixed 7 d later. In control neurons, the GFP-fluorescence is dim and diffuse, indicative of GFP quenching in acidified late endosomes/lysosomes. As expected, the mCherry fluorescence is bright, as this fluorophore does not quench in acidic environments. In PFF-treated neurons, the GFP fluorescence is bright and punctate, indicating that the fluorophore was not quenched and thus that the late endosomes/lysosomes are not acidified properly. Scale bar, 10 μm. (D) The relative size of Lamp1 puncta was quantified from the confocal images. The data did not pass a normality test. The scatter plot of the median and interquartile range reveals an increase in the larger Lamp1 endosomes in α-syn aggregate–bearing neurons. Mann–Whitney test, $p < 0.0001$. (E) Percentage overlap of LC3 with LAMP1 quantified from confocal images. The data fit a normal distribution. There was a statistically significant decrease in the overlap of LC3 autophagosomes with LAMP1 late endosomes/lysosomes ($t(23) = 4.275$, $p = 0.0003$).

was substantially reduced. We previously demonstrated an overall increase in autophagy markers in cells and neurons with α-syn inclusions, with a decrease in autophagic flux (Tanik *et al.*, 2013). Here we detect clear decreases in the normal acidification of autophagolysosomes in the soma of α-syn aggregate–bearing neurons and reduced colocalization of LC3 with LAMP1, suggesting impaired autophagosome/lysosome fusion. Previous findings showed that pharmacological treatments that impair endosome/lysosome pro-

teolysis or acidification cause selective defects in axon transport (Lee *et al.*, 2011). Defects in autophagosome function could cause neurodegeneration (Nixon, 2013). In our neuron-based model of a-syn inclusion formation, we do not observe cell death until 2 wk after PFF exposure. It is likely that because autophagosome transport is not completely abolished (indeed, the autophagosomes that remain mobile have increased velocities), the cumulative impairments in autophagosome transport and function over time ultimately lead to a

progressive reduction in neuron function and, ultimately, neuron death.

What could account for the selective decreases in axonal transport? Lipid composition distinguishes distinct membrane organelles, and aberrant interaction of α-syn with membranes may contribute to their impaired transport. The results that support this possibility are as follows. First, α-syn is normally associated with acidic phospholipid–containing membranes through interaction of its amino-terminal heptad repeats with membrane lipids (Davidson *et al.*, 1998; Westphal and Chandra, 2013). Second, α-syn has been shown to associate with endosomes and lysosomes, and increased accumulation of α-syn at these membrane structures perturbs their morphology (Rockenstein *et al.*, 2005; Boassa *et al.*, 2013). Third, studies in yeast overexpressing α-syn demonstrate an accumulation of endosomes and impaired membrane traffic (Gitler *et al.*, 2008; Soper *et al.*, 2008, 2011). Further, whereas in vitro studies demonstrate nonselective association of α-syn with acidic phospholipids, it is possible that in vivo, α-syn, particularly the misfolded form, associates with phosphatidylinositol-3-phosphate and phosphatidylinositol 3,5-bisphosphate, phosphoinositides enriched in endosomes and in which impaired metabolism has been linked to neurodegenerative diseases (Gillooly *et al.*, 2000; Rutherford *et al.*, 2006; Volpicelli-Daley and De Camilli, 2007).

Association of α-syn with select adaptors and scaffolding proteins involved in axonal transport may also cause the distinct effects of the inclusions on endosome/autophagosome transport. For example, neurotrophin-induced phosphorylation of dynein IC-1B is crucial for the transport of TrkB receptors and Rab7 but not mitochondria (Mitchell *et al.*, 2012). Snapin has also been shown to be a selective adaptor for transport of TrkB- and Rab7-containing endosomes and for autophagosomes/lysosomes (Cai *et al.*, 2010; Zhou *et al.*, 2012). Future experiments will determine whether α-syn inclusions sequester any adaptors or scaffolding proteins selectively involved in late endosome and autophagosome transport.

In conclusion, our findings demonstrate that aberrant axonal transport may be one of the mechanisms that leads to impaired neural transmission and ultimately cell death in synucleinopathies such as PD. Altered transport of endosomes and autophagosomes could lead to cell death by altering signaling pathways associated with cell survival, lead to an accumulation of damaged proteins and organelles, and impair neuronal function. Moreover, because different strains of α-syn PFFs can also cross-seed the recruitment of the microtubule-associated protein tau (Guo *et al.*, 2013), it will be of great interest whether aggregates of different compositions can produce distinct and even more profound effects on axonal transport. Finally, we now add pathological accumulations of α-syn to the growing list of gene products implicated in PD that alter endosome/lysosome/autophagosome pathways, such as glucocerbrosidase (Mazzulli *et al.*, 2011), lysosomal type 5 P-type ATPase (Dehay *et al.*, 2012; Usenovic *et al.*, 2012), leucine-rich repeat kinase-2, and Rab7L1 (Macleod *et al.*, 2013), and it is possible that altered transport of these organelles may be a common feature contributing to the etiology of this disease.

MATERIALS AND METHODS
Reagents
Timed pregnant CD1 mice were obtained from Charles River (Wilmington, MA), and α-syn KO mice were obtained from the Jackson Laboratory (Bar Harbor, ME). GFP was ligated in-frame at the C-terminus of α-syn and cloned into the pcDNA3.1 vector to generate the α-syn–GFP plasmid. Other plasmid constructs include APP-YFP (Kaether *et al.*, 2000), synaptophysin-GFP (Kaether *et al.*,

2000), and pEYFP-Mito (Clontech, Mountain View, CA). The following plasmids (followed by plasmid number) were obtained from Addgene (Cambridge, MA): GFP-Rab7 (12605), mRFP-Rab7 (14436), GFP-LC3 (21073), TrkB-GFP (32500), RFP-Ub (11935), and mCherry-GFP-LC3 (22418).

Primary neuronal cultures and transfections
All procedures were performed according to the National Institutes of Health Guide for the Care and Use of Experimental Animals and were approved by the University of Pennsylvania Institutional Animal Care and Use Committee. Dissociated hippocampal neurons were plated onto poly-D-lysine–coated coverslips in a 24-well plate (1×10^4/well) or MatTek dishes (MatTek Ashland, MA) at 5×10^5 cells/dish. Neurons were cultured in neuronal medium (Neurobasal medium, B27, GlutaMAX; Life Technologies, Grand Island, NY) without penicillin/streptomycin. Neurons were transfected with various cDNAs using Lipofectamine 2000 (Life Technologies) 4 d after plating. For one MatTek dish, a total of 1 μg of plasmid DNA was diluted in 50 μl of prewarmed DMEM (Life Technologies), and 1 μl of Lipofectamine 2000 was diluted into 50 μl of DMEM and allowed to incubate at 25°C for 5 min. The DNA/DMEM and Lipofectamine 2000/DMEM were mixed and incubated at 25°C for 20 min and then added directly to the medium in each dish. Four hours later, the entire medium was exchanged for a 50/50 mixture of conditioned and fresh neuronal media.

PFF treatment
Full length, wild-type α-syn PFFs were prepared, and neurons were treated with 5 μg/ml PFF at DIV5 as described previously (Volpicelli-Daley *et al.*, 2011, 2014).

Live imaging
Imaging was performed 7 d after adding PFFs at 37°C, 5% CO_2, with buffer containing 136 mM NaCl, 2.5 mM KCl, 2 mM $CaCl_2$, 1.3 mM $MgCl_2$, 10 mM glucose, and 10 mM 4-(2-hydroxyethyl)-1-piperazineethanesulfonic acid. For BDNF treatments, neurons were treated with 50 ng/ml BDNF (PeproTech, Rocky Hill, NJ) for 1 h before imaging. BDNF was also included in the imaging buffer. Epifluorescence imaging was performed with a Nikon TE-2000-E (Nikon, Tokyo, Japan) inverted microscope with a 60× oil immersion objective. Regions of thin axons at least 100 μm away from growth cones or adjacent cell bodies were chosen. Unless otherwise stated in the figure legends, images were captured every second for a total of 3 min at 300-ms exposure time. Spinning disk confocal images were captured with an Olympus IX81 (Center Valley, PA) inverted microscope and an iXon3 electron-multiplying charge-coupled device camera (Andor, South Windsor, CT) at the University of Pennsylvania Cell and Developmental Biology Microscopy Core Facility. Scanning confocal microscopy was performed using a TCS SP5 Visible-Upright Confocal Microscope (Leica Microsystems, Buffalo Grove, IL) at the University of Alabama-Birmingham Center for Neurodegeneration and Experimental Therapeutics.

Image analysis
Image analysis was performed using ImageJ (National Institutes of Health, Bethesda, MD). Kymographs from individual axons were generated, and average velocities were determined manually using the kymographs. All of the lines generated in the kymograph were used in the analyses, and none were rejected. Average velocity was determined by drawing a line from the beginning of a particle trajectory to the end, measuring total distance traveled and total time

traveled, and the average velocity was calculated as total distance divided by total time (Supplemental Figure S1). Mobile vesicles were defined as puncta that move 0.1 μm/s (e.g., 20 μm over 3 min). Reversals were counted as a reversal in direction of movement for ≥5 μm. A pause counted as movement of <0.1 μm/s at any point during the trajectory of a mobile vesicle. Data were analyzed using SPSS software (IBM, Armonk, NY) or Prism (GraphPad, La Jolla, CA). Because the velocities for all experiments did not fit a normal distribution (as determined by the D'Agostino and Pearson omnibus normality test), the velocity data were analyzed using Poisson regression on velocities binned with 10 cut points. The Mann–Whitney or Kruskal–Wallis test was also used to test for significant differences among groups. In the case of analyzing the number of particles per 50-μm membrane, the velocities fit a normal distribution, and thus an independent t test was performed.

Electron microscopy

Transmission electron microscopy and immunolabeling with HRP or immunogold electron microscopy for p-α-syn inclusions using the mAb 81A (Waxman and Giasson, 2008) were performed as described previously (Volpicelli-Daley et al., 2011). Primary neurons were grown on Thermanox plastic coverslips (Electron Microscopy Sciences, Hatfield, PA). Neurons were fixed in 2.5% glutaraldehyde in 0.1 M cacodylate buffer, pH 7.4, and postfixed for 1 h in 1% OsO_4 and 1.5% potassium ferrocyanide in 0.05 M cacodylate buffer. Images were captured using a Jeol 1010 electron microscope (Jeol, Peabody, MA) at the University of Pennsylvania's Biomedical Imaging Core.

Immunofluorescence

Immunofluorescence was performed as described previously (Volpicelli-Daley et al., 2011). Briefly, neurons were fixed with 4% paraformaldehyde/4% sucrose or 4% paraformaldehyde/4% sucrose/1% Triton X-100 in PBS, followed by permeabilization and blocking with 0.1% Triton X-100/3% bovine serum albumin. Neurons were incubated in primary antibodies, followed by Alex Fluor–conjugated secondary antibodies (Life Technologies, Carlsbad, CA). Primary antibodies include mAb 81A (Waxman and Giasson, 2008), LAMP1 (1D4B; Developmental Studies Hybridoma Bank, University of Iowa, Iowa City, IA), NeuN (MAB377; EMD Millipore, Billerica, MA), and pERK5 (sc-16564; Santa Cruz Biotechnology, Dallas, TX).

REFERENCES

Boassa D, Berlanga ML, Yang MA, Terada M, Hu J, Bushong EA, Hwang M, Masliah E, George JM, Ellisman MH (2013). Mapping the subcellular distribution of alpha-synuclein in neurons using genetically encoded probes for correlated light and electron microscopy: implications for Parkinson's disease pathogenesis. J Neurosci 33, 2605–2615.

Braak H, Del Tredici K, Rub U, de Vos RAI, Steur ENHJ, Braak E (2003). Staging of brain pathology related to sporadic Parkinson's disease. Neurobiol Aging 24, 197–211.

Braak H, Sandmann-Keil D, Gai W, Braak E (1999). Extensive axonal Lewy neurites in Parkinson's disease: a novel pathological feature revealed by alpha-synuclein immunocytochemistry. Neurosci Lett 265, 67–69.

Cai Q, Li L, Tian J-H, Zhu Y-B, Qiao H, Sheng Z-H (2010). Snapin-regulated late endosomal transport is critical for efficient autophagy-lysosomal function in neurons. Neuron 68, 73–86.

Chandra S, Fornai F, Kwon HB, Yazdani U, Atasoy D, Liu X, Hammer RE, Battaglia G, German DC, Castillo PE, Sudhof TC (2004). Double-knock-out mice for alpha- and beta-synucleins: effect on synaptic functions. Proc Natl Acad Sci USA 101, 14966–14971.

Davidson WS, Jonas A, Clayton DF, George JM (1998). Stabilization of alpha-synuclein secondary structure upon binding to synthetic membranes. J Biol Chem 273, 9443–9449.

Decressac M, Kadkhodaei B, Mattsson B, Laguna A, Perlmann T, Bjorklund A (2012). alpha-Synuclein-induced down-regulation of Nurr1 disrupts GDNF signaling in nigral dopamine neurons. Sci Transl Med 4, 163ra156.

Dehay B, Ramirez A, Martinez-Vicente M, Perier C, Canron MH, Doudnikoff E, Vital A, Vila M, Klein C, Bezard E (2012). Loss of P-type ATPase ATP13A2/PARK9 function induces general lysosomal deficiency and leads to Parkinson disease neurodegeneration. Proc Natl Acad Sci USA 109, 9611–9616.

Deinhardt K, Salinas S, Verastegui C, Watson R, Worth D, Hanrahan S, Bucci C, Schiavo G (2006). Rab5 and Rab7 control endocytic sorting along the axonal retrograde transport pathway. Neuron 52, 293–305.

Duda JE, Giasson BI, Mabon ME, Lee VM, Trojanowski JQ (2002). Novel antibodies to synuclein show abundant striatal pathology in Lewy body diseases. Ann Neurol 52, 205–210.

Duffy PE, Tennyson VM (1965). Phase and electron microscopic observations of Lewy bodies and melanin granules in substantia nigra and locus coeruleus in Parkinson's disease. J Neuropathol Exp Neurol 24, , 398–414.

Ferrer I, Blanco R, Carmona M, Puig B, Barrachina M, Gomez C, Ambrosio S (2001). Active, phosphorylation-dependent mitogen-activated protein kinase (MAPK/ERK), stress-activated protein kinase/c-Jun N-terminal kinase (SAPK/JNK), and p38 kinase expression in Parkinson's disease and dementia with Lewy bodies. J Neural Transm 108, 1383–1396.

Forno LS, Norville RL (1976). Ultrastructure of Lewy bodies in the stellate ganglion. Acta Neuropathol 34, 183–197.

Giasson BI, Duda JE, Quinn SM, Zhang B, Trojanowski JQ, Lee VM (2002). Neuronal alpha-synucleinopathy with severe movement disorder in mice expressing A53T human alpha-synuclein. Neuron 34, 521–533.

Gillooly DJ, Morrow IC, Lindsay M, Gould R, Bryant NJ, Gaullier JM, Parton RG, Stenmark H (2000). Localization of phosphatidylinositol 3-phosphate in yeast and mammalian cells. EMBO J 19, 4577–4588.

Gitler AD, Bevis BJ, Shorter J, Strathearn KE, Hamamichi S, Su LJ, Caldwell KA, Caldwell GA, Rochet JC, McCaffery JM, et al. (2008). The Parkinson's disease protein alpha-synuclein disrupts cellular Rab homeostasis. Proc Natl Acad Sci USA 105, 145–150.

Guo JL, Covell DJ, Daniels JP, Iba M, Stieber A, Zhang B, Riddle DM, Kwong LK, Xu Y, Trojanowski JQ, Lee VM (2013). Distinct alpha-synuclein strains differentially promote tau inclusions in neurons. Cell 154, 103–117.

Hayashida K, Oyanagi S, Mizutani Y, Yokochi M (1993). An early cytoplasmic change before Lewy body maturation: an ultrastructural study of the substantia nigra from an autopsy case of juvenile parkinsonism. Acta Neuropathol 85, 445–448.

Kaether C, Skehel P, Dotti CG (2000). Axonal membrane proteins are transported in distinct carriers: a two-color video microscopy study in cultured hippocampal neurons. Mol Biol Cell 11, 1213–1224.

Kimura S, Noda T, Yoshimori T (2007). Dissection of the autophagosome maturation process by a novel reporter protein, tandem fluorescent-tagged LC3. Autophagy 3, 452–460.

Kopito RR (2000). Aggresomes, inclusion bodies and protein aggregation. Trends Cell Biol 10, 524–530.

Kramer ML, Schulz-Schaeffer WJ (2007). Presynaptic alpha-synuclein aggregates, not Lewy bodies, cause neurodegeneration in dementia with Lewy bodies. J Neurosci 27, 1405–1410.

Lee MK, Stirling W, Xu Y, Xu X, Qui D, Mandir AS, Dawson TM, Copeland NG, Jenkins NA, Price DL (2002). Human alpha-synuclein-harboring familial Parkinson's disease-linked Ala-53 –> Thr mutation causes neurodegenerative disease with alpha-synuclein aggregation in transgenic mice. Proc Natl Acad Sci USA 99, 8968–8973.

Lee S, Sato Y, Nixon RA (2011). Lysosomal proteolysis inhibition selectively disrupts axonal transport of degradative organelles and causes an Alzheimer's-like axonal dystrophy. J Neurosci 31, 7817–7830.

Lewis TB, Standaert DG (2010). Parkinson's disease, primate, and gene therapy: vive la difference? Mov Disord 26, 2–3.

Macleod DA, Rhinn H, Kuwahara T, Zolin A, Di Paolo G, Maccabe BD, Marder KS, Honig LS, Clark LN, Small SA, Abeliovich A (2013). RAB7L1 Interacts with LRRK2 to modify intraneuronal protein sorting and Parkinson's disease risk. Neuron 77, 425–439.

Maday S, Wallace KE, Holzbaur EL (2012). Autophagosomes initiate distally and mature during transport toward the cell soma in primary neurons. J Cell Biol 196, 407–417.

Masliah E, Rockenstein E, Veinbergs I, Mallory M, Hashimoto M, Takeda A, Sagara Y, Sisk A, Mucke L (2000). Dopaminergic loss and inclusion body formation in alpha-synuclein mice: implications for neurodegenerative disorders. Science 287, 1265–1269.

Mazzulli JR, Xu YH, Sun Y, Knight AL, McLean PJ, Caldwell GA, Sidransky E, Grabowski GA, Krainc D (2011). Gaucher disease glucocerebrosidase and alpha-synuclein form a bidirectional pathogenic loop in synucleinopathies. Cell 146, 37–52.

McNaught KS, Shashidharan P, Perl DP, Jenner P, Olanow CW (2002). Aggresome-related biogenesis of Lewy bodies. Eur J Neurosci 16, 2136–2148.

Mitchell DJ, Blasier KR, Jeffery ED, Ross MW, Pullikuth AK, Suo D, Park J, Smiley WR, Lo KW, Shabanowitz J, et al. (2012). Trk activation of the ERK1/2 kinase pathway stimulates intermediate chain phosphorylation and recruits cytoplasmic dynein to signaling endosomes for retrograde axonal transport. J Neurosci 32, 15495–15510.

Morfini GA, Burns M, Binder LI, Kanaan NM, LaPointe N, Bosco DA, Brown RHJr, Brown H, Tiwari A, Hayward L, et al. (2009). Axonal transport defects in neurodegenerative diseases. J Neurosci 29, 12776–12786.

Nixon RA (2013). The role of autophagy in neurodegenerative disease. Nat Med 19, 983–997.

Perlson E, Maday S, Fu MM, Moughamian AJ, Holzbaur EL (2010). Retrograde axonal transport: pathways to cell death? Trends Neurosci 33, 335–344.

Rockenstein E, Schwach G, Ingolic E, Adame A, Crews L, Mante M, Pfragner R, Schreiner E, Windisch M, Masliah E (2005). Lysosomal pathology associated with alpha-synuclein accumulation in transgenic models using an eGFP fusion protein. J Neurosci Res 80, 247–259.

Roy S, Winton MJ, Black MM, Trojanowski JQ, Lee VM (2007). Rapid and intermittent cotransport of slow component-b proteins. J Neurosci 27, 3131–3138.

Rutherford AC, Traer C, Wassmer T, Pattni K, Bujny MV, Carlton JG, Stenmark H, Cullen PJ (2006). The mammalian phosphatidylinositol 3-phosphate 5-kinase (PIKfyve) regulates endosome-to-TGN retrograde transport. J Cell Sci 119, 3944–3957.

Salinas S, Bilsland LG, Schiavo G (2008). Molecular landmarks along the axonal route: axonal transport in health and disease. Curr Opin Cell Biol 20, 445–453.

Soper JH, Kehm V, Burd CG, Bankaitis VA, Lee VM (2011). Aggregation of alpha-synuclein in S. cerevisiae is associated with defects in endosomal trafficking and phospholipid biosynthesis. J Mol Neurosci 43, 391–405.

Soper JH, Roy S, Stieber A, Lee E, Wilson RB, Trojanowski JQ, Burd CG, Lee VM (2008). Alpha-synuclein-induced aggregation of cytoplasmic vesicles in Saccharomyces cerevisiae. Mol Biol Cell 19, 1093–1103.

Tanik SA, Schultheiss CE, Volpicelli-Daley LA, Brunden KR, Lee VM (2013). Lewy body-like alpha-synuclein aggregates resist degradation and impair macroautophagy. J Biol Chem 288, 15194–15210.

Usenovic M, Tresse E, Mazzulli JR, Taylor JP, Krainc D (2012). Deficiency of ATP13A2 leads to lysosomal dysfunction, alpha-synuclein accumulation, and neurotoxicity. J Neurosci 32, 4240–4246.

Valdez G, Akmentin W, Philippidou P, Kuruvilla R, Ginty DD, Halegoua S (2005). Pincher-mediated macroendocytosis underlies retrograde signaling by neurotrophin receptors. J Neurosci 25, 5236–5247.

Volpicelli-Daley L, De Camilli P (2007). Phosphoinositides' link to neurodegeneration. Nat Med 13, 784–786.

Volpicelli-Daley LA, Luk KC, Lee VM (2014). Addition of exogenous α-synuclein preformed fibrils to primary neuronal cultures to seed recruitment of endogenous α-synuclein to Lewy body and Lewy neurite-like aggregates. Nat Protoc 9, 2135–2146.

Volpicelli-Daley LA, Luk KC, Patel TP, Tanik SA, Riddle DM, Stieber A, Meaney DF, Trojanowski JQ, Lee VM (2011). Exogenous alpha-synuclein fibrils induce Lewy body pathology leading to synaptic dysfunction and neuron death. Neuron 72, 57–71.

Watanabe I, Vachal E, Tomita T (1977). Dense core vesicles around the Lewy body in incidental Parkinson's disease: an electron microscopic study. Acta Neuropathol 39, 173–175.

Watson FL, Heerssen HM, Bhattacharyya A, Klesse L, Lin MZ, Segal RA (2001). Neurotrophins use the Erk5 pathway to mediate a retrograde survival response. Nat Neurosci 4, 981–988.

Waxman EA, Giasson BI (2008). Specificity and regulation of casein kinase-mediated phosphorylation of alpha-synuclein. J Neuropathol Exp Neurol 67, 402–416.

Westphal CH, Chandra SS (2013). Monomeric synucleins generate membrane curvature. J Biol Chem 288, 1829–1840.

Xie Z, Klionsky DJ (2007). Autophagosome formation: core machinery and adaptations. Nat Cell Biol 9, 1102–1109.

Zhou B, Cai Q, Xie Y, Sheng ZH (2012). Snapin recruits dynein to BDNF-TrkB signaling endosomes for retrograde axonal transport and is essential for dendrite growth of cortical neurons. Cell Rep 2, 42–51.